

An Interactive Deformable Model Segmentation Algorithm Driven by Morphological Dilations and Erosions Constrained by an Exclusion Band

Marcos Carneiro de Andrade ¹

Centro de Desenvolvimento da Tecnologia Nuclear – CDTN, P.O. Box 970, Belo Horizonte, MG Brazil.

Received 4th Jan 2011; accepted on 05th Dec 2012

Abstract

This study introduces an interactive image segmentation algorithm for extraction of ill-defined edges (faint, blurred or partially broken) often observed at small-scale imaging. It is based on a simplified deformable elastic model evolution paradigm. Segmentation is achieved as a two-step region-growing, shrinking and merging simulation constrained by an exclusion band built around the edges of the regions of interest, defined from a variation image. The simulation starts from a set of unlabeled markers and the respective elastic models. During the first step, model evolution occurs entirely outside the exclusion band, driven by alternate action-reaction movements. Forward and backward movements are performed by constrained binary morphological dilations and erosions. Constraints allow controlling how far models can move through narrow gaps. At the end of the first step, models remaining from merging operations receive unique and exclusive labels. On the second and final step, models expansion occurs entirely inside the exclusion band, now driven only by binary unconstrained morphological dilations. A point where two labeled models get into contact defines an edge point. The simulation goes on until the concurrent expansion of all models comes to a complete stop. At this point, the edges of the regions-of-interest have been extracted. Interactivity introduces the possibility to correct small imperfections in the edge positioning by changing a parameter controlling action-reaction or by changing marker's size, position and shape. Slightly inspired by traditional approaches as PDE Level-Set based curve evolution and Immersion Simulation, the algorithm presents a solution to the problem of “synchronizing the concurrent evolution of a large number of models” and an “automatic stopping criterion” for the front propagation. Integer arithmetic implementation assures linear execution time. The results obtained for real applications show that even ill-defined edges can be located with the desired accuracy, thanks to algorithm features and to the interactivity exerted by the user during the segmentation procedure.

Key Words: Image segmentation, front propagation, elastic models, denoising, microscopy, nanoscopy

1. Introduction

Some materials, when observed at microscopic or nanoscopic scale reveal a structure compound of a periodic network of nearly polygonal regions separated by thin edges, as shown in the examples presented in Figure 1. Important structural properties as, for example, 2D or 3D particle size

¹ Correspondence to: marcos.c.de.andrade@gmail.com

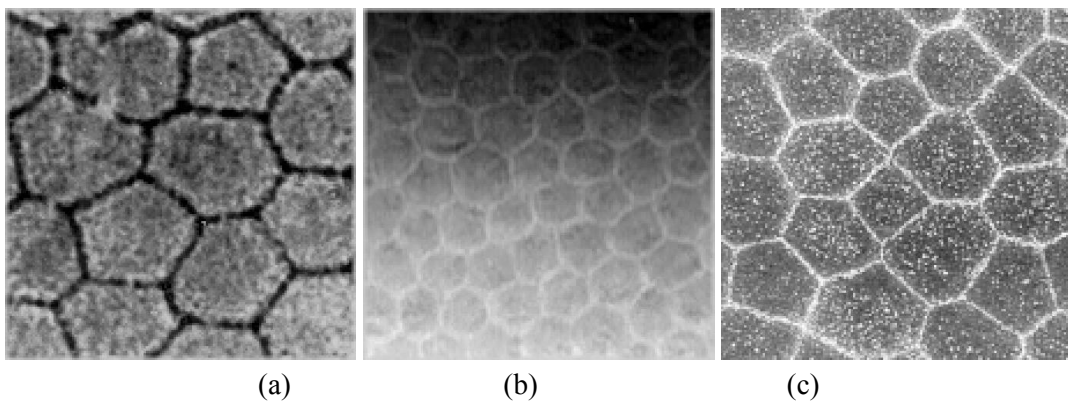
Recommended for acceptance by F. Perales

ELCVIA ISSN: 1577-5097

Published by Computer Vision Center by Universitat Autònoma de Barcelona, Barcelona, Spain.

distribution can be determined from these small-scale images. To yield reliable statistical information a robust image segmentation algorithm is required to extract with sufficient accuracy the edges of a large number of regions-of-interest (ROIs). In this context, accuracy means the algorithm ability to extract the edges of the ROIs with relative fidelity, i.e., the edges must be closed, thin (~1 pixel wide) and located as close as possible to the real object's boundaries, even if the boundaries of the objects are ill-defined (faint, blurred or partially broken).

Limitations related to material formation, sample preparation and image acquisition processes defy automated image segmentation at small-scale. The 15 sample images shown in Figure 1 illustrate some of these limitations. All these images present regions delimited by ill-defined edges of variable degree of complexity. Figures 1a, 1b and 1c show, respectively, layers of cells of corneal endothelial tissue of a bovine, a human and a yacare eye. The cells in these micrographs show non-homogeneous illumination, noise and partially broken boundaries. Micrographs 1d, 1e and 1f reveal the microstructure of leaves organized in a hierarchy of small, medium and large domains of *different* thicknesses containing a mix of complete and incomplete structures with blurred edges. Micrograph 1g shows a pollen grain containing regions separated by spaces whose thicknesses vary a lot. The clearly perceptible non-homogeneous illumination results from the curvature of the grain surface. Micrograph 1h shows corrosion pitches and noise in a sheet of stainless steel. When computing size distributions for a large number of pitches, a careful noise removal strategy is required to avoid changing pitch's surface areas. In 1i a nanograph of a thin magnetic film shows blurred transversal tracks which may lead to incorrect edge extraction. The samples of ceramic material shown in 1j, 1k and 1l contain grains (homogeneous surface), pores (small dots) and twins (thin straight lines crossing from one side to the other). Pores may appear inside grains and over the edges, making edge detection harder. If the segmentation algorithm is not robust enough, twins may be taken by edges. The same is true for patterns of light and dark regions, resulting from internal stress, shown in micrograph 1l. Samples of stainless steel shown in 1m, 1n and 1o, contain respectively, twins inside grains, partially blurred edges of variable thickness and individual grains reflecting light in different directions as a result of uneven leveling, making grains to appear in different false colors.



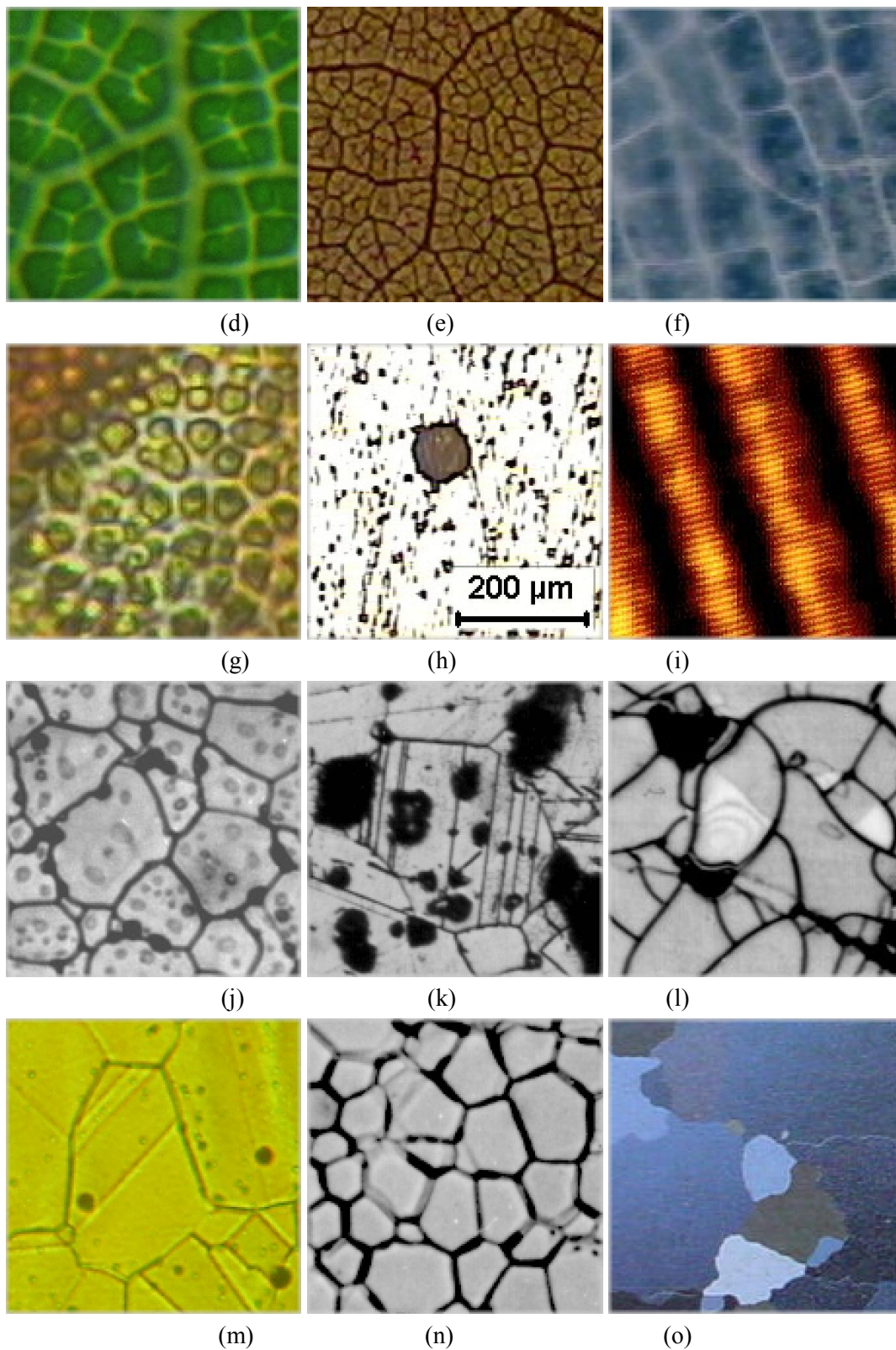


Figure 1. Examples of nano and microstructures with polygonal shapes separated by thin edges.

A careful observation of these images shows that the above mentioned issues clearly require careful denoising and segmentation strategies to yield reliable results.

The image segmentation literature encompasses a large variety of approaches, ranging from artificial intelligence as Genetic and Evolutionary Computing [16], Fuzzy Clustering and Neural Discrimination [18], [22] to classical region-growing based methods as, for instance, Seeded Region Growing [14], Watershed Transformation [01, 02], Level-Set Method [03,04,05].

Applications of particular interest here are the segmentation at nanoscopic scale imaging [21], grain edge extraction [20], and corneal endothelial cells [15].

Broadly classified into two distinct categories, edge extraction methods can try direct edge detection or to extract edges indirectly by a region-growing process. For direct edge detection approach, refer to the compilation recently prepared by Papari and Petrov [06].

Despite the large variety of methods available in the literature, here we are particularly interested in region-growing based methods, in especial non-linear ones, because they allow fine control over the processes involved the region formation, expansion, shrinking and merging. Some important non-linear region-growing methods are based on simulation of physical phenomena as *Immersion Simulation* [01, 02] and *Deformable Models Driven by Action-Reaction Forces* [03, 04, 05].

An ideal edge detector should have the ability to extract the edges of the ROIs even in presence of faint, blurred or partially broken boundaries and to yield completely closed edges, having preferably 1 pixel width, located as close as possible to the “real” boundaries of the objects. These requirements are necessary to allow assessment of geometric parameters as surface areas, perimeters, form factor, etc. The approach presented in this paper, Interactive Deformable Model Segmentation Algorithm for Small Scale Imaging - IDMSA is an attempt to mitigate the above mentioned problems.

2. The Interactive Deformable Model Segmentation Algorithm for Small Scale Imaging - IDMSA.

The original motivation behind this approach was to develop a set of algorithms to extract the edges of corneal endothelial cells for veterinary applications [13] (see fig. 1a to 1c) and the edges of ceramic oxide grains for applications in nuclear industry (see fig. 1j to 1l). Despite being of very different nature these materials share many features related to the segmentation problem. In both cases, cells and grains fill most of the image field and are separated by tiny boundaries. A closer look to these images reveals that the most important pixels, from the segmentation point of view, are situated exactly inside a narrow band (a few pixels wide) containing the edges of the ROIs, from now on, called the “exclusion band” or EB.

IDMSA algorithm can be viewed as a non-linear region-growing simulating the concurrent expansion, contraction and merging of a set of deformable elastic models which, at the end of the process, envelop the boundaries of the ROIs. The simulation is a two-step process driven by binary morphological dilations and erosions constrained by set of displacement rules. During the first step, models grow, shrink and merge exclusively outside the EB. The EB synchronizes the progression of models, retaining the fast marching models close to its boundaries, giving time to slower ones to arrive. The initial expansion continues until all elastic models completely stop, converging to the boundaries of the EB. During this step, action-reaction parameters control the model’s ability to penetrate into narrow gaps. All topological changes required to merge non-significant regions occurs spontaneously as models get into contact. A second and final expansion occurs exclusively inside the

EB, at this time driven only by unconstrained morphological dilations, until they finally stop close to the edges of the ROIs.

To assure fast execution and linear run time the segmentation algorithm resorts only to integer arithmetic. Interactivity allows improving the final location of the extracted edges within the expected accuracy. The algorithm has been tested with success for different real applications as shown in Section 3.

2.1 IDMSA steps

IDMSA algorithm is executed in the following consecutive steps:

1. *Denoising the original image.*
2. *Computation of a local variation image from the original image.*
3. *Definition of an “exclusion band” around the edges of the ROIs in the variation image.*
4. *Insertion of one or more marker per ROI by hand and/or by an automated process.*
5. *First propagation of the elastic deformable models outside the EB.*
6. *Labeling markers with consecutive and positive integer labels.*
7. *Second and final propagation of the labeled deformable elastic models inside the EB.*
8. *Edge extraction from the labeled image.*

Before the first expansion starts (step 5) all image pixels outside the EB are marked as “non-processed”. During the first propagation, all “non-processed” points and their immediate neighborhood are visited at least once. Despite local contractions, the net model’s movement is always expanding away from markers. After some iteration, all models converge to the edges of the EB. In step 7, the evolution occurs inside the EB in an ever-expanding movement (no contraction). Again, each unlabelled pixel and its neighbourhood are visited at least once, assuring the convergence of the whole process.

2.1.1 Image Denoising for Markers Extraction

Before discussing and illustrating the strengths of denoising for markers extraction, it should be anticipated that there is no general-purpose denoising strategy applicable to all kind of image. Usually a given class of image can be denoised by a pre-defined sequence of filters, which once defined can be applied to the whole class. Moreover, each particular application will require a specialized strategy to extract markers. The reason is that non-linear filtering responds quite differently and is strongly dependent on parameters. For example, the effect of Alternated Sequential Filters (ASF) and Geodesic Erosion and Dilation, two powerful morphological filters, depend on the structuring element size, shape, number of iterations and of the image features.

In the current approach, denoising serves mainly to reduce the number of local minima to be used as markers for each region-of-interest (ROI).

The following examples show a sequence of denoising operations performed by a fully automated procedure for a sample of corneal endothelial cells [13]. Figure 2a shows an original micrograph (left) of *in vitro* corneal endothelial cells of yacare eye with no filtering and the corresponding local minima (right). Notice the large number of local minima (small dots) regularly distributed along the image field. In the sequence, it is shown how different denoising strategies of increasing complexity and performance, applied to the image shown in Figure 2a, can change the number, shape, size and spatial

of local minima, viz: mean filter (b), mean filter followed by median filter (c), mean filter followed by geodesic erosion [07] filter (d) and mean filter followed by alternated sequential [08] filter (e).

IDMSA does not require a single marker per ROI, since multiple models evolving from the respective markers, inside a ROI, will lately be merged into a single model representing that ROI. Indeed the more the number of markers the faster models will converge.

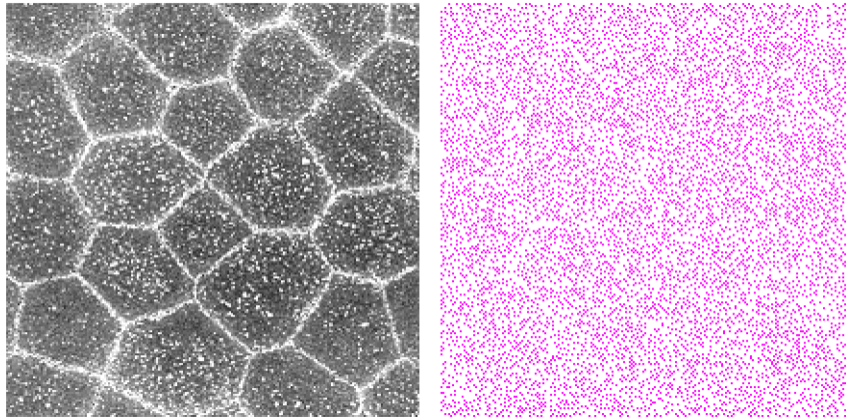


Figure 2a. Original micrograph of corneal endothelial cells and its local minima.

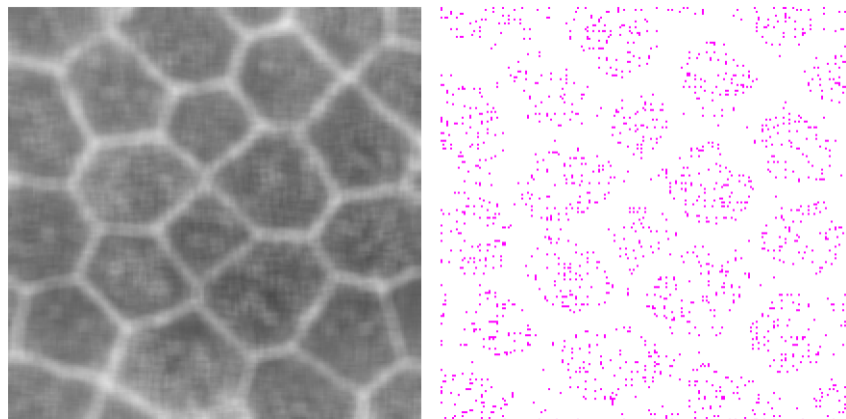


Figure 2b. Effect of a 7x7 mean filter and its local minima.

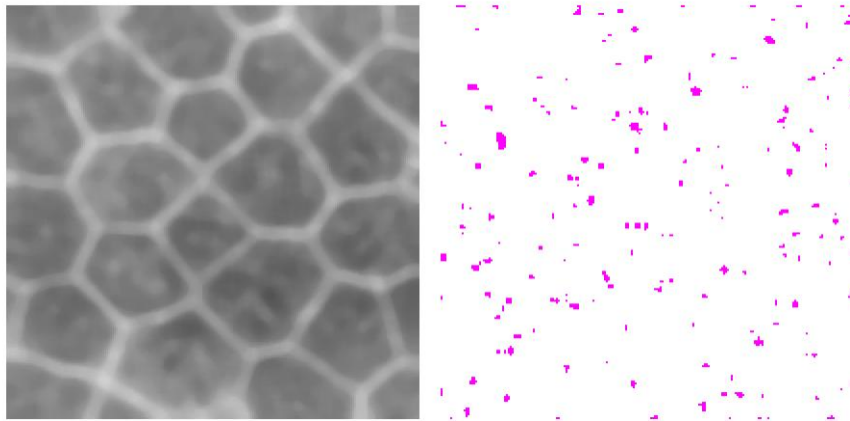


Figure 2c. Effect of mean and median filters and its local minima.

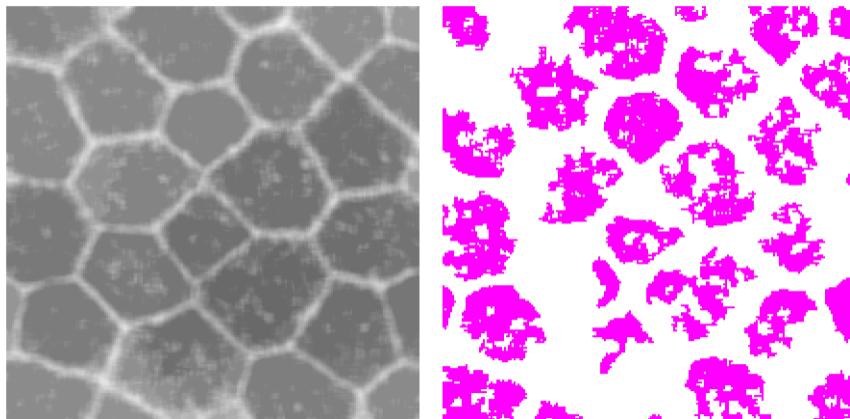


Figure 2d. Effect of mean and geodesic erosion filters and its local minima.

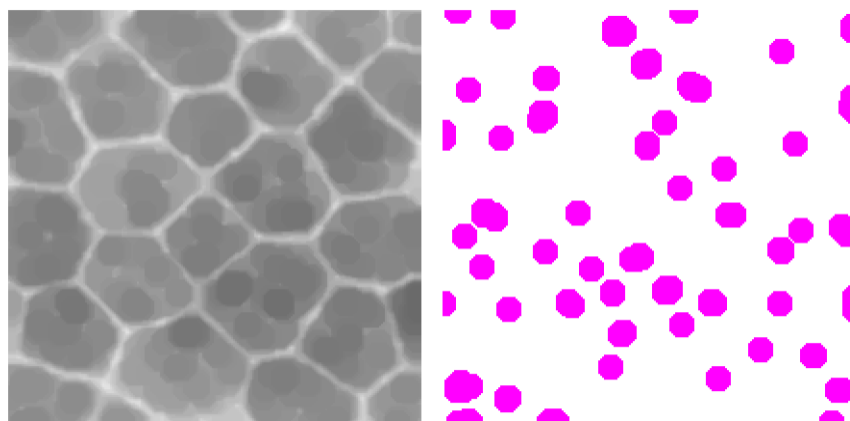


Figure 2e. Effect of mean and ASF and its local minima.

A continuous improvement is clearly perceptible by comparing the filtering sequences (b) to (e). It becomes evident that a careful denoising strategy must be defined to get a suitable set of markers.

2.1.2 Defining a set of markers and the corresponding elastic models

Sometimes a large number of markers is required to segment an image. In these cases, it may be virtually impossible to extract hundreds or even thousands of markers by hand. Therefore, a fully automated markers extraction is usually followed by a manual edition, in which, minor corrections are introduced in the set of markers. As previously shown in Section 2.1.1, automated sequences of specialized filters are the method of choice in IDMSA to extract markers. However, a parameterized grid may be a useful alternative to get the set of initial field of markers. A parameterized grid does not depend on local extrema (maxima or minima) and may yield much denser field of markers. Figure 3 illustrates how a set of markers can be defined for a layer of corneal endothelial cells using a parameterized grid in a fully automated process. The points of the grid are set on and off depending on pairs of experimental thresholds, set for background ($th1 = 5.0$, $th2 = 100.0$) and foreground ($th1 = 0.05$, $th2 = 1.0$). These values hold for any image of this class. The average local intensity m for each grid point p , the corresponding standard deviation s , and the variation coefficient $c_{var} = s/m$, are computed on a square neighborhood $N(p)$ of size k around p . A grid point is set “on” if $th1 \leq c_{var} \leq th2$, otherwise it is set “off”. Figure 3a shows a grid of square markers for grid pitch (point density) = 6 pixels and marker size = 3 pixels superimposed on a gray scale image of corneal endothelial cells. Figure 3b shows a grid of markers defined for pitch = 12 and size = 5.

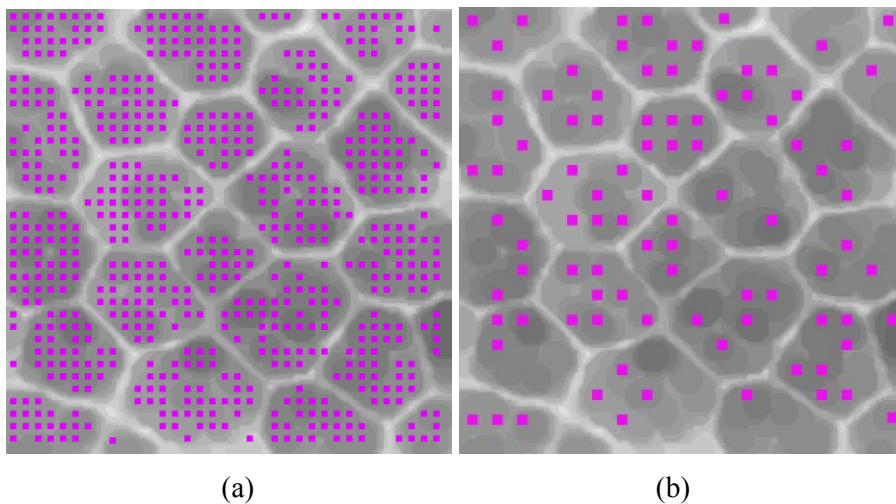


Figure 3. Marker set by a parameterized grid and threshold.

An especial “frame marker” shown in pink in Figure 4a was used to discard incomplete features (background) located on the boundaries of the image field. In Figure 4b green dots represent regions-of-interest (foreground) and the pink dots represent non-significant regions (background).

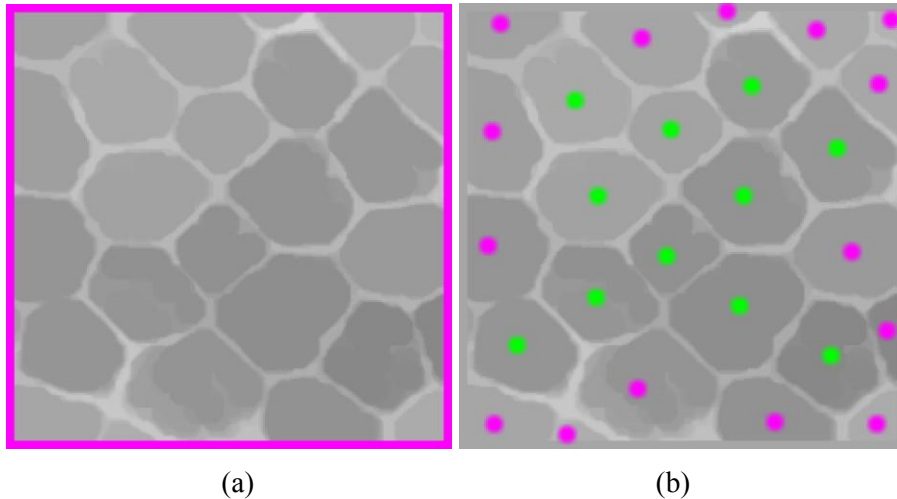
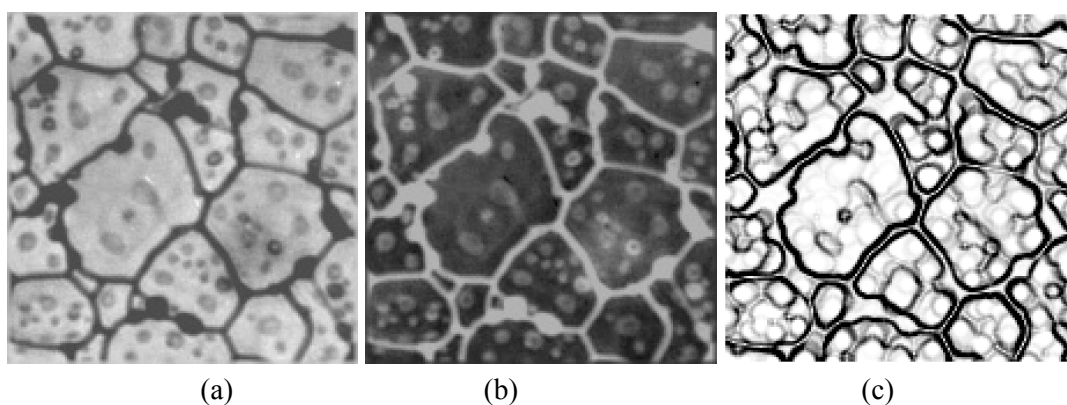


Figure 4. (a) Frame marker around the image field, (b) markers for relevant and irrelevant cells.

Before the second model expansion (step 7) starts all models are labeled with exclusive integer numbers. Connected component labeling is a straightforward operation and will not be discussed here. Refer to a linear time connected component labeling algorithm introduced by Chang [11] and a much simpler but non-linear time algorithm described in Gonzalez et al. [12].

2.1.3 Computation of a Total Variation (TV) image.

Local variation images present strong intensity changes near the edges of the objects, a feature explored by IDMSA. Figure 5 shows alternative instances of local variation images: the negative image (b), the gradient image (c), the morphological gradient image (d), the local curvature image (e) [09] and the Total Variation image (TV) (f) [10]. Choosing a particular variation image may depend on the features involved but, in general, the TV image shows edges with relatively better definition and is preferable in IDMSA.



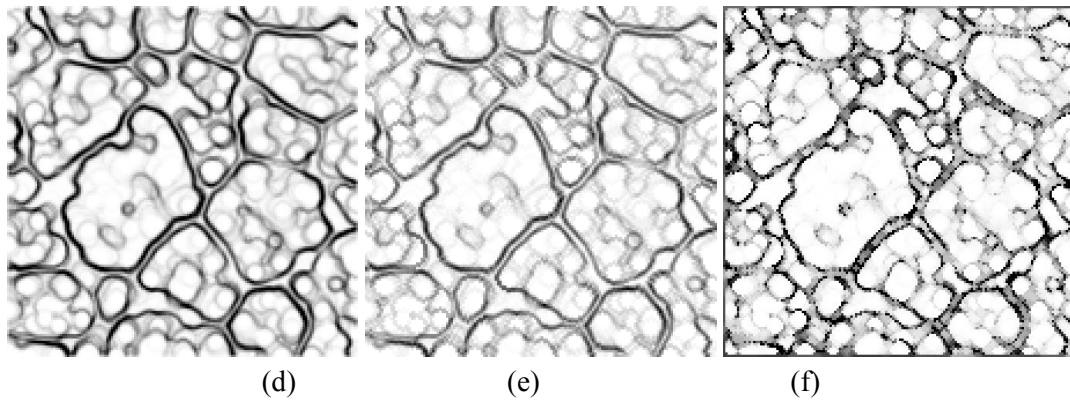


Figure 5. Instances of local variation images for the original image shown in (a): (b) negative, (c) gradient by Sobel, (d) total variation (TV), (e) morphological gradient, (f) local curvature.

2.1.4 Definition of an exclusion band (EB) around the TV image.

Figure 6 shows EBs computed from TV images for real and synthetic images. A user-selected threshold Th sets the thickness of EB. A point p pertains to the EB if $\text{abs}(I(p) - mp) > Th$.

Where: $I(p)$ is the image intensity at point p .

$N(p)$ is an arbitrary neighborhood of size $k \times k$ around point p .

mp is the average image intensity in $N(p)$.

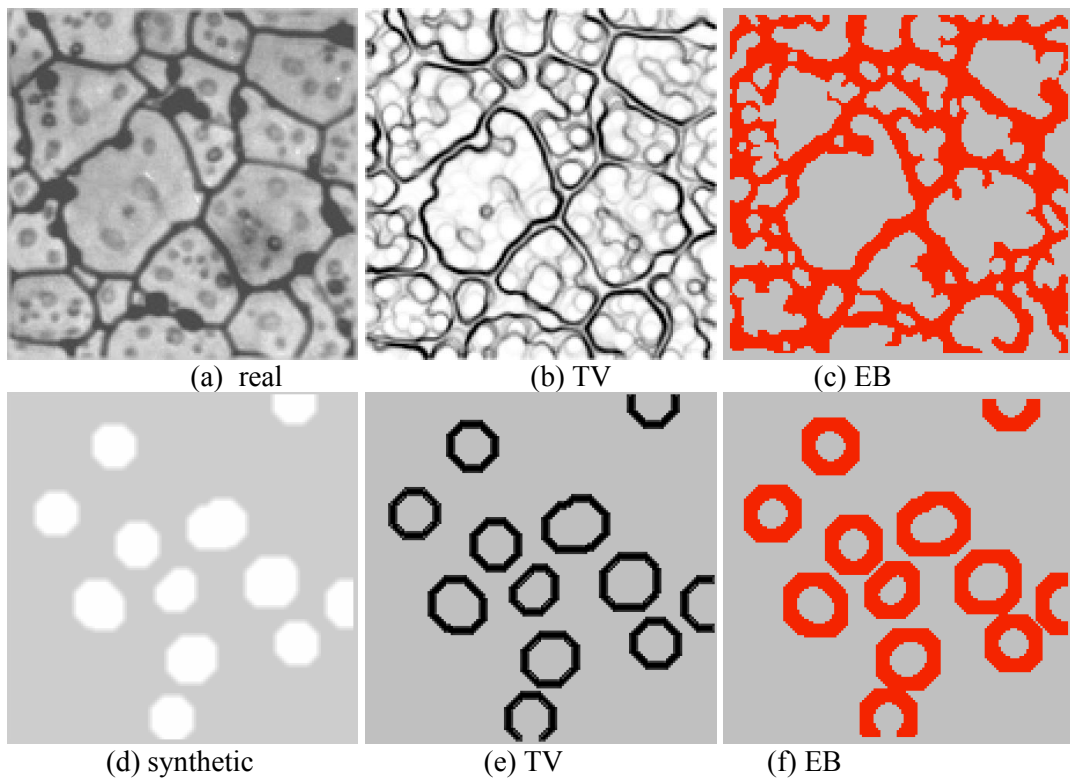


Figure 6. TV and EB images for a real ceramic sample and a synthetic blob images.

The frames shown in Figure 7 illustrate how an intensity threshold Th , applied to a synthetic gray level image of blobs, affects the EB thickness. Clearly, thresholds like $Th = 5$ or $Th = 45$ are more restrictive to model displacement and yield thicker bands; conversely less restrictive thresholds would lead to comparatively narrower EBs. In this example, thresholds above 80 are useless since several contact points appear between the inner and outer edges of the EB, compromising it as a stopping barrier for the evolving elastic models. Thicker EBs may lead to less precise edge location, which by its turn may require further changes in the set of markers.

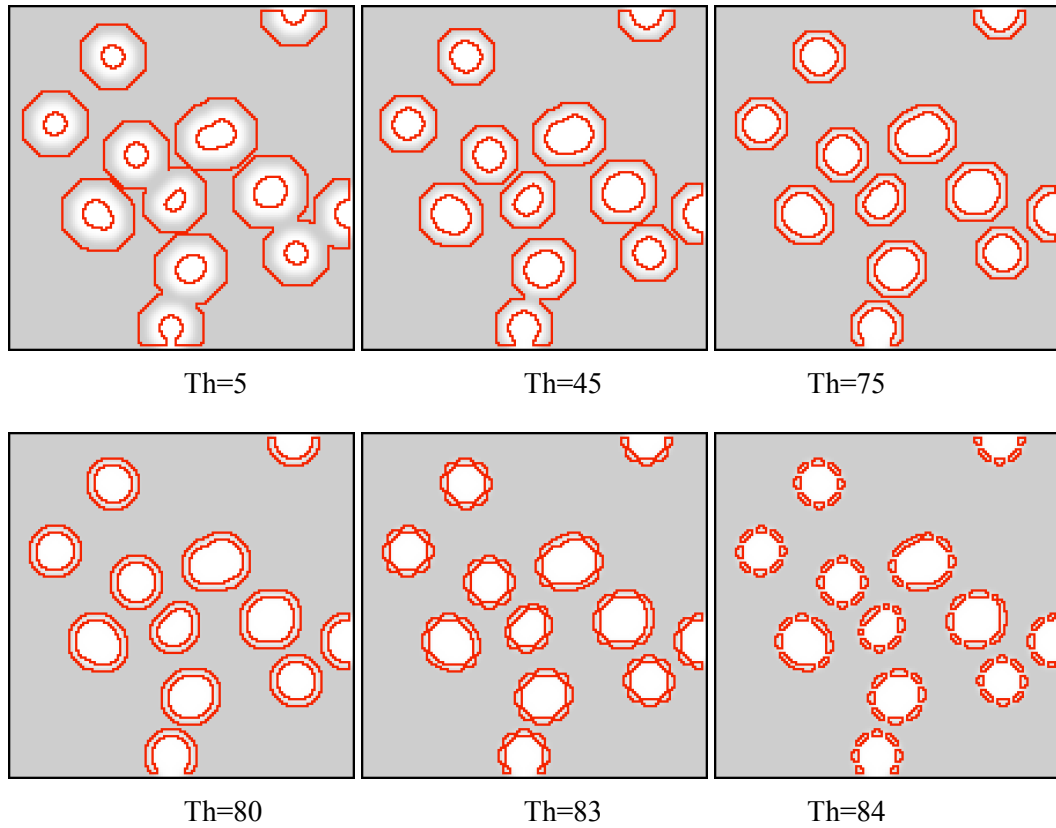


Figure 7. EB thickness as a function of increasing thresholds applied on the TV image.

2.1.5 Model growing, shrinking and merging.

2.1.2.1 Growing and Shrinking

Model growing and shrinking were implemented as action and reaction pairs of consecutive and competing movements driven by binary dilation and erosion operators. Action represents model growing while reaction may represent both growing and shrinking, depending on the set of rules defined below:

Action as a conditional binary dilation:

if $(p \notin Eb) \wedge (p > 0) \wedge (\exists p+) \wedge (\exists p-)$ set p to -1 .

Reaction as conditional binary erosion:

if $(p \in Eb) \wedge (p < 0) \wedge (Sp \geq 0)$ set p to $+1$;

Reaction as a conditional binary dilation:

if $(p \in Eb) \wedge (p > 0) \wedge (Sp < 0)$ set p to -1 .

Where,

p^-	point of negative polarity in $N(p)$, i.e., a pixel belonging to a marker;
p^+	point of positive polarity in $N(p)$, i.e., a pixel not yet processed;
Sp	the sum of all labeled points (positive and negative) around p , except p itself;
EB	exclusion band around the edges, i.e., $EB = \{ p \in Iv \mid (Iv(p) - Iav(p)) > Th \}$;
Th	an intensity threshold;
Iv	a local variation image;
$Iv(p)$	variation image intensity at point p ;
Iav	variation image average intensity in $N(p)$.
$N(p)$	neighborhood of size 3 around p .

2.1.5.2 Merging

Merging results from the collapse of two or more unlabeled models into a unique model. It occurs during the first expansion step exclusively outside the EB and responds for changes in the topology of the evolving models.

Two binary buffers $i1$ and $i2$ were used to implement the models evolution. Markers and background received initially the following signal assignment:

- a negative polarity (-) to all points belonging to markers.
- a positive polarity (+) to all other image points.

Changes in polarity may occur as models evolve. After the initial marker assignment, action is performed in buffer $i1$, which is then copied to buffer $i2$, then reaction is computed into buffer $i2$, which is copied back to buffer $i1$. This sequence is repeated, forcing models to move outward, until idempotence is achieved, i.e., there is no difference between the two buffers.

In Figure 8, a schematic diagram represents windows at arbitrary time t and $t+1$, containing 16×16 points, cut from the binary buffers $i1$ and $i2$ and used to perform the segmentation. Individual markers are represented by gray closed regions containing positive (-) signed point, delimited elastic models shown as thin blue lines. Unprocessed points are represented by negative (-) signed points. Bold face type (red) indicates a change of polarity for action-reaction pair for two consecutive instants of time t and $t+1$.

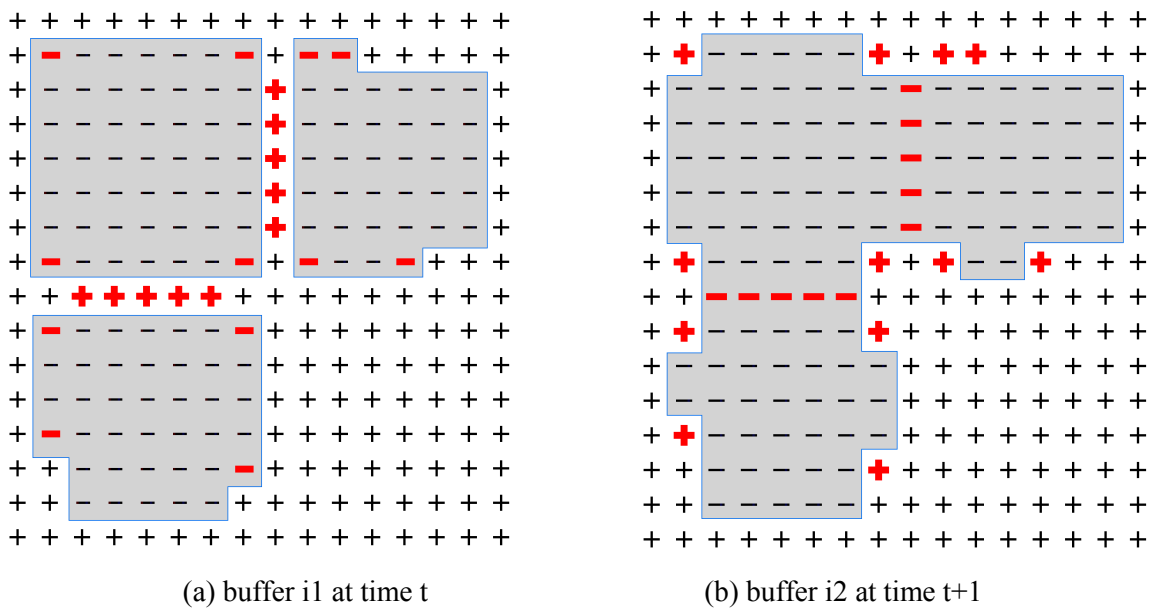


Figure 8. Red signs indicate change of polarity for two consecutive instants of time.

Figure 9 illustrates how action-reaction parameters are used to exert fine control over the models displacement. Figure 10a shows a synthetic image containing ROIs represented by bars (white) separated by thin edges (gray) whose thicknesses vary from 1 to a few pixels wide. The EB (orange) and a set of arbitrary markers (pink) are also shown. Figures 9b and 9c illustrate the elastic model ability to get into narrow gaps under the effect of action alone and action plus reaction, respectively. The elastic models (thin red closed lines) locations are represented as a function of time t , at the initial (t_i) after a few interactions (t_k) and final time (t_f).

As illustrated, the EB acts as a barrier blocking the displacement of the elastic models beyond its boundaries. An additional restriction to the elastic model displacement is exerted by reaction, which during the first front propagation step, blocks the movement parallel to and also over narrow edges. Compare the shape and the corresponding model penetration ability of the models into narrow gaps for situations (action alone) and (action plus reaction) respectively in Figures 9b and 9c.



Figure 9a. Synthetic thin edges of increasing thickness (gray), the corresponding EB (orange) and an arbitrary set of markers (pink).

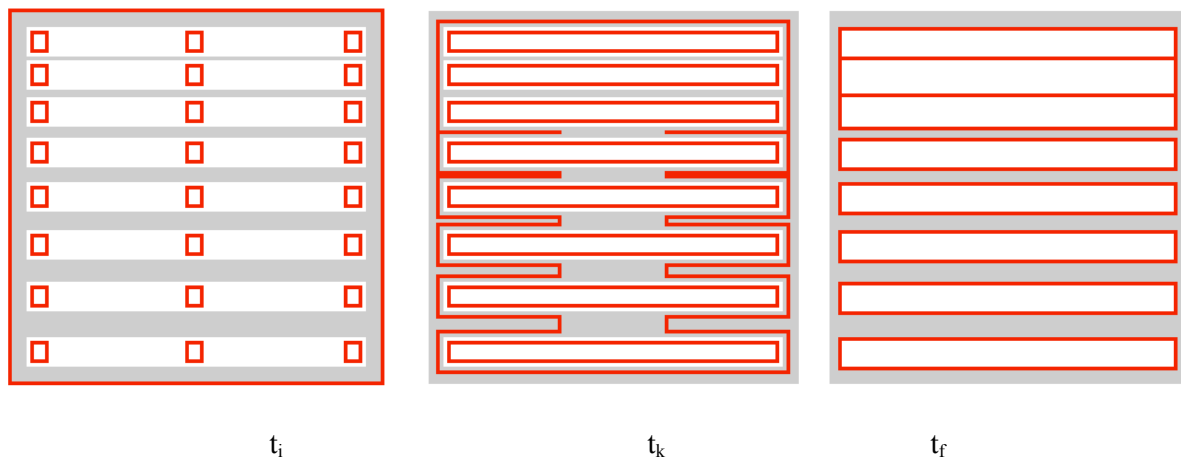


Figure 9b. Model ability to get into narrow gaps as a function of action.

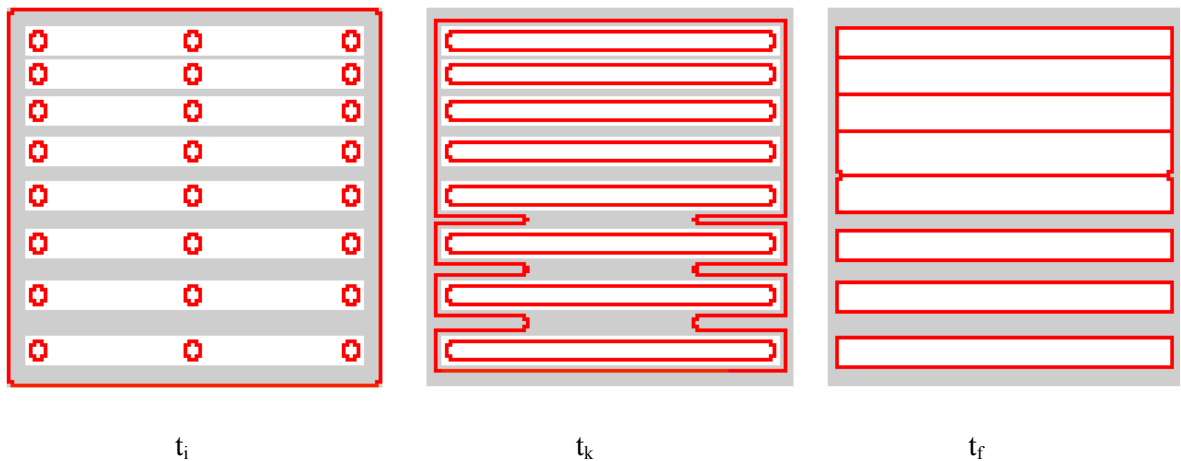


Figure 9c. Model ability to get into narrow gaps as a function of action and reaction.

Action performs a conditional binary dilation by a $k \times k$ structuring element by expanding the model at most 1 pixel per iteration. Reaction performs a conditional binary erosion and/or dilation by a $k \times k$ structuring element. A forward movement of the deformable model inside thin narrow gaps (a few pixels wide) may be completely undone by a backward movement. These alternate growing and shrinking movements have a final effect of blocking the model progression and, therefore, prevent leaking through thin gaps. The EB by its turn blocks movement perpendicular to broken or faint edges.

Arrows in Figure 10 show an elastic model expanding in directions parallel and over the edges of a cell (b) or leaking through a broken edge (c); situations that can be minored or completely avoided in IDMSA by tuning the EB thickness and turning reaction on.

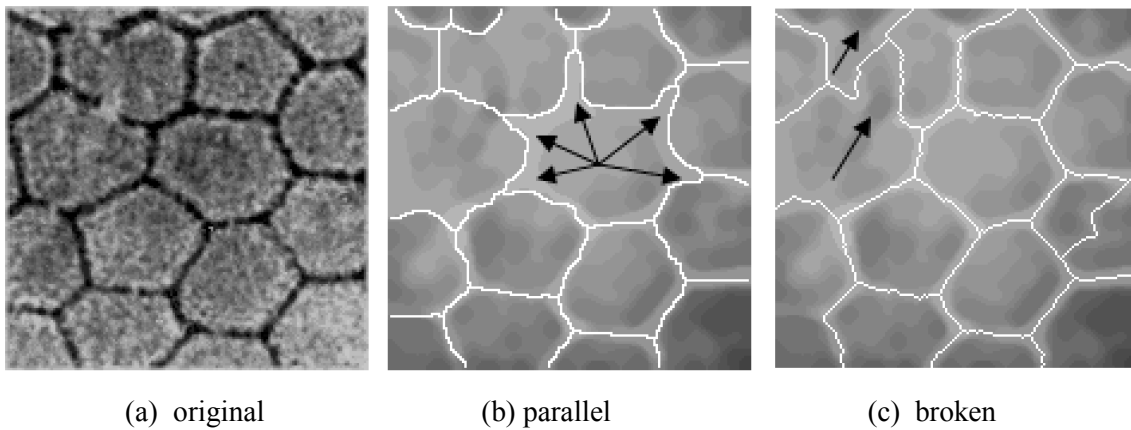
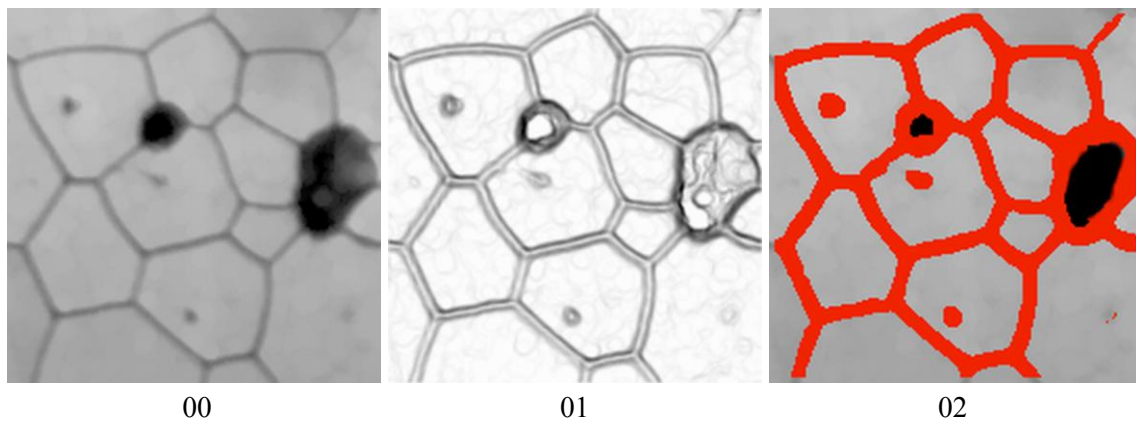
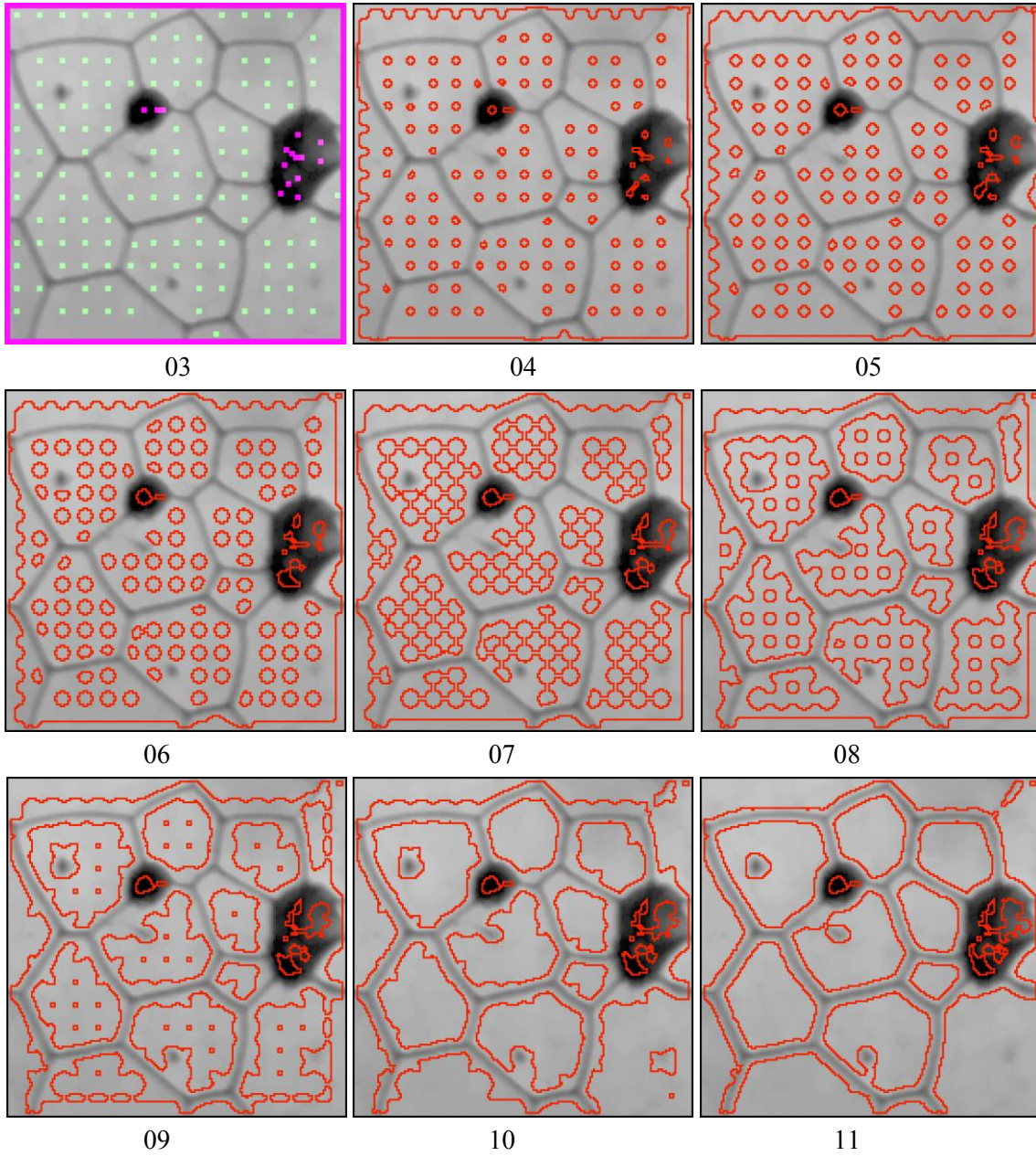


Figure 10. Model growing parallel and over the edge and leaking through broken edges.

2.1.6 Model evolution at different stages of IDMSA

The snapshots shown in Figure 11 illustrate the evolution of the elastic models for 16 consecutive segmentation steps. The original image of a ceramic material containing grains and pores is shown in frame 00. Frame 01, 02 and 03 show respectively the total variation image computed from the original image, the EB image computed from the TV image and a set of markers for grains, pores (foreground) and incomplete grains (background). A thin square marker shown at snapshot 03 was used to discard incomplete cells on the borders of the image field. Frames 4 to 12 represent snapshots of the first stage in the evolution of the elastic models. At frame 12 all models have achieved idempotence for the first time, i.e., there is no more difference between two successive instants in the evolution. At this instant each model receives a unique integer label. Frames 13 to 15 represent snapshots of the second evolution stage without merging and/or contraction. From instant 13 on, only growing of labeled models is allowed. It stops where two or more models get into contact, therefore defining an edge point. Snapshot 15 shows the final segmentation result. Animations of the models in evolution can be downloaded from the ELCVIA site.





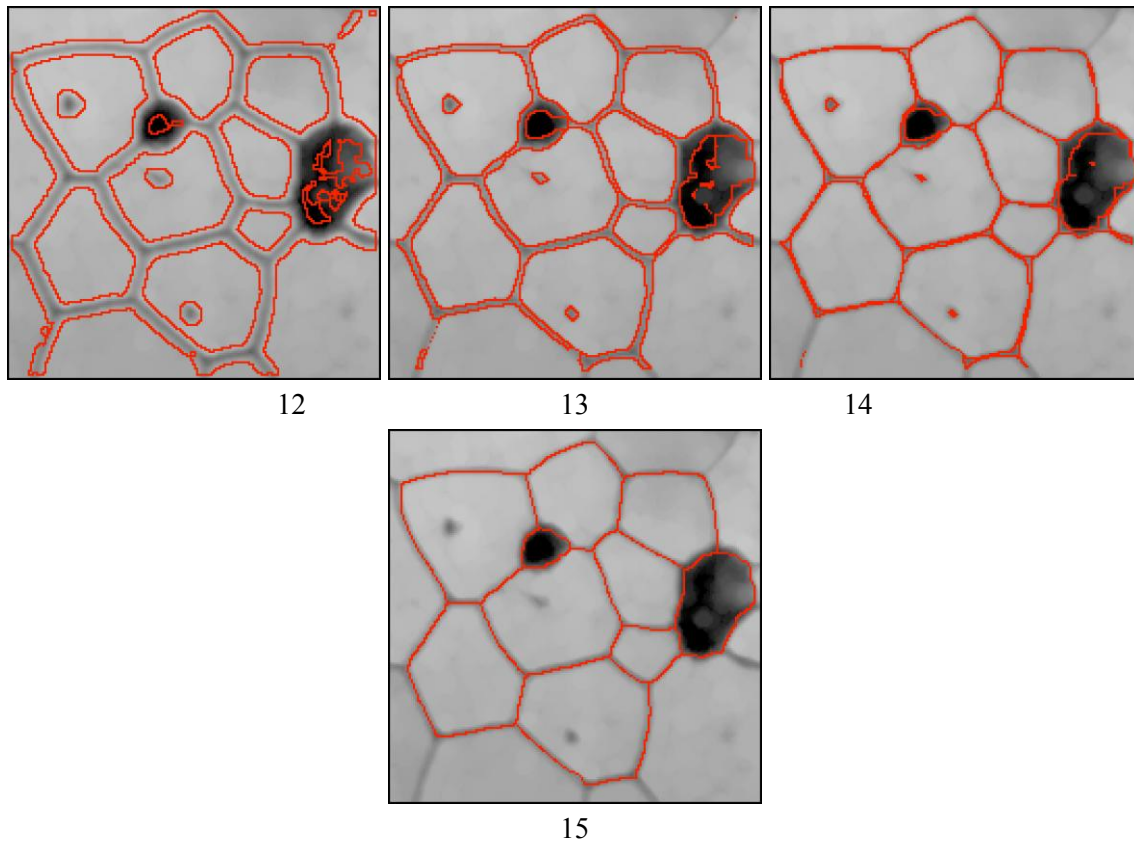


Figure 11. Models in evolution at different stages of IDMSA segmentation.

3. Applications

All images presented in this section were obtained from real applications. The material samples shown in Figures 12a to 12d have different nature and structure, but surprisingly share many similarities regarding the problems faced during the segmentation task. These images reveal a structure compound of nearly polygonal objects separated by thin, blurred, broken or incomplete boundaries, which must be correctly extracted to allow the assessment of geometrical and statistical parameters without bias. For example, a reliable assessment of the histogram of area distribution depends on the accurate extraction of closed contour for each object.

Figure 12a shows an optical micrograph of a ceramic material containing grains (polygons) separated by thin boundaries (dark lines) and pores (dark spots). Very few pores are present inside each individual grain. Figure 12b show a similar material having many inner pores, which should not be taken into account by the segmentation algorithm. Figure 13c shows an optical micrograph of a biological sample containing a very thin layer of corneal endothelial cells of a yacare eye. The assessment of the cells size distribution may serve as a clue to corneal endothelial transplant. Finally, the nanograph presented in Figure 12d shows parallel magnetic tracks on a thin film whose edges are to be extracted to allow the assessment of their relative surface density in the image field. As shown in these images, the final position of the elastic models (thin red contours) is very close to the real boundaries of the objects, thanks to the IDMSA evolution strategy. A combination of a mechanism to synchronize the evolving models and another to stop front propagation is responsible for the results

achieved. Minor correction in the final position of models may be done by slightly changing the set of markers.

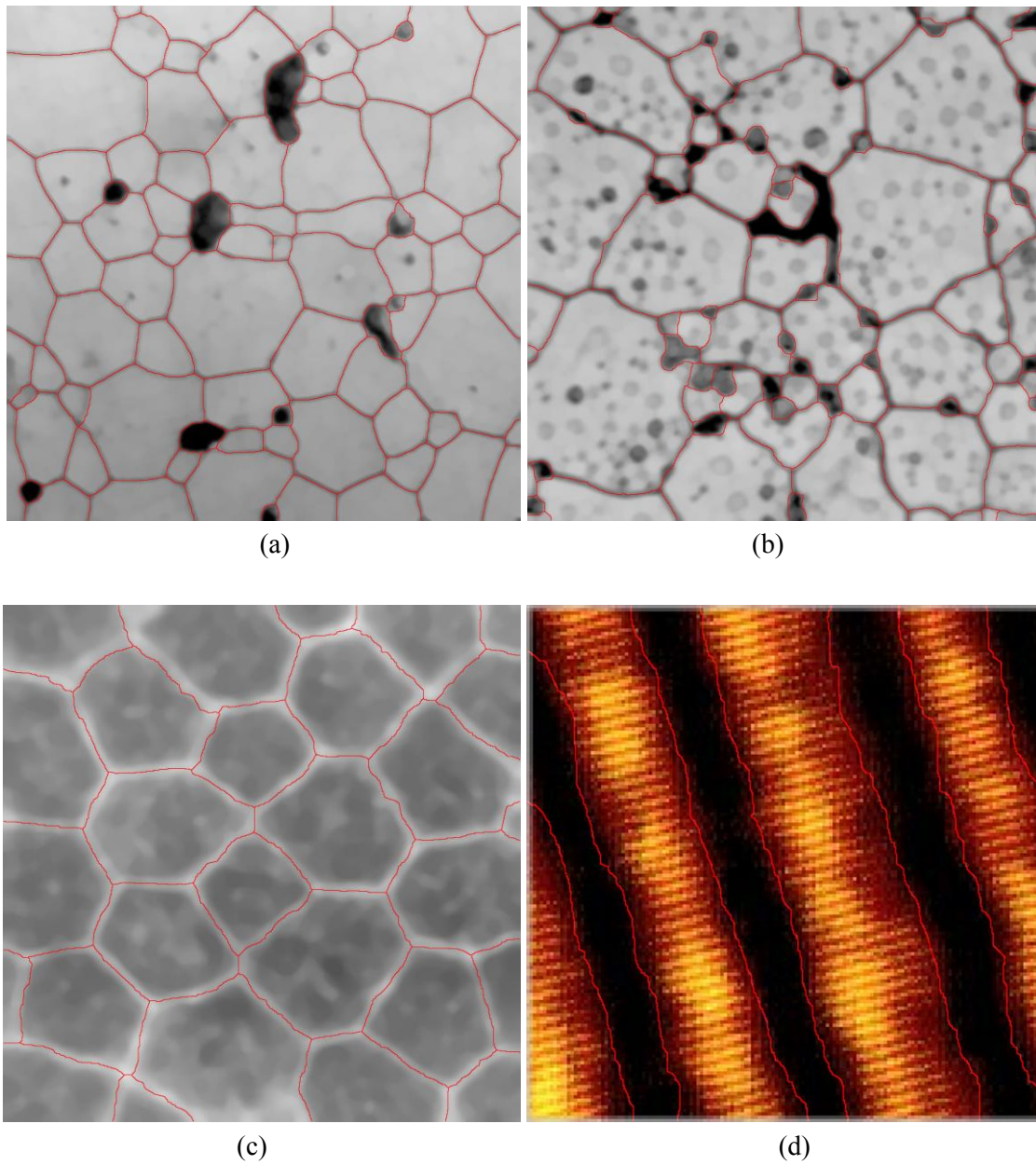


Figure 12. Examples of IDMSA segmentation for micro and nano structured materials.

4. Discussion

Before discussing pros and cons of the IDMSA approach it is worth to present some important features of closely related segmentation methods. *Immersion simulation* is a non-linear region-growing technique, in which a large number of models grow in parallel starting from local or regional minima towards the edges of the objects. Non-linearity stems from the topographic information, which dictates the order of processing. This feature provides an intrinsic and automated mechanism to synchronize all regions growing in parallel. Immersion Simulation is highly sensitive to minor variation in the local topography. During an immersion simulation all local minima are detected and gives rise to an associated catchment basin. Of course, a suitable set of markers must be defined to avoid the well known over-segmentation problem, illustrated in Figure 13a.

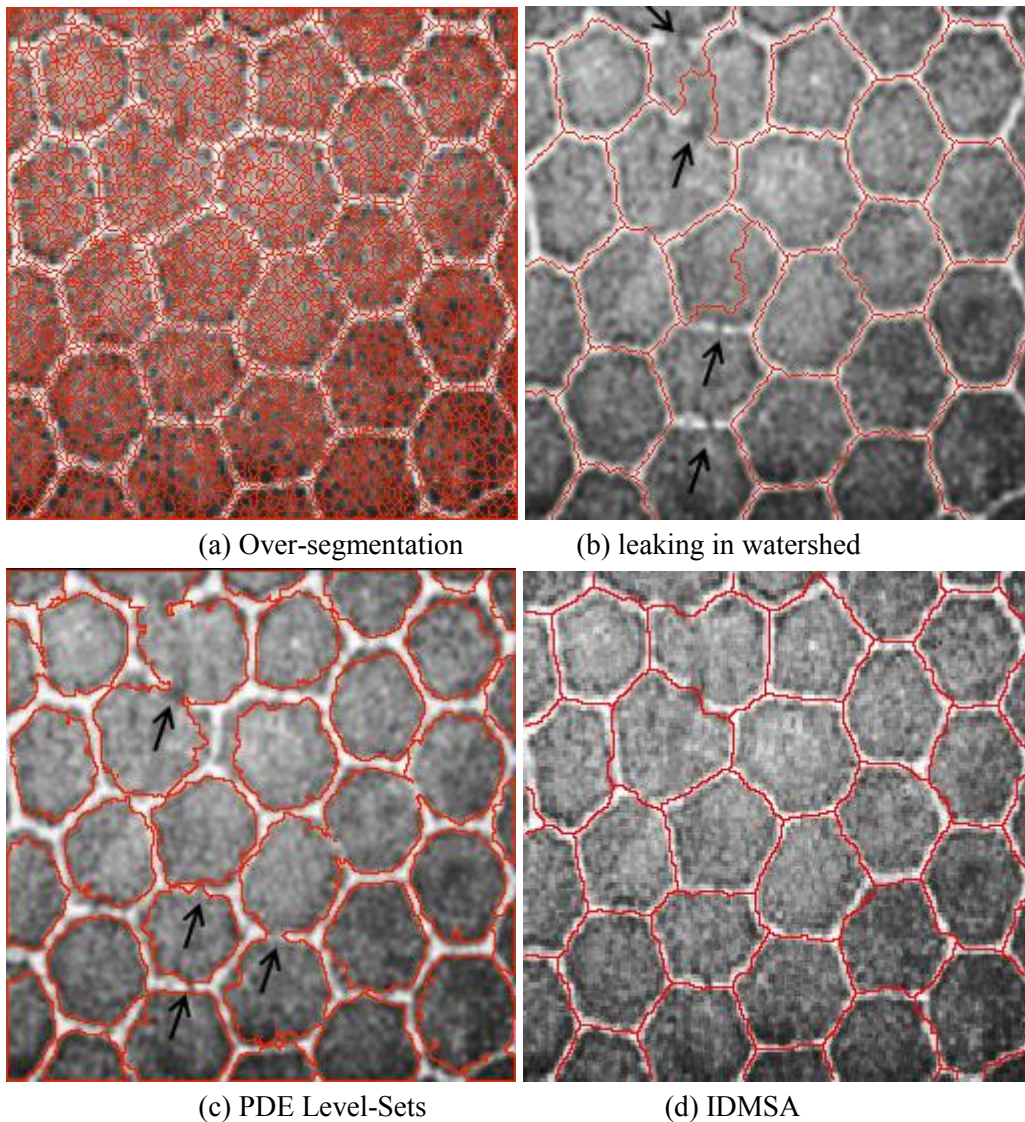


Figure 13. Problems found in segmentation of thin, faint, blurred and broken-edges.

This same sensitivity to the local topography, provides the immersion simulation with an excellent ability to stop the region growing evolution over faint or blurred edges but, unfortunately, cannot avoid leaking through partially broken boundaries, as shown by arrows in Figure 13b.

A gap on the edge is sufficient to let models “leak”. Leaking occurs because a broken boundary introduces a topographic change, which ultimately modifies the order of processing, i.e. the hierarchy of processing.

On the other hand, methods based on *Deformable Models Driven by PDEs* as the Level-Sets Method can stop the evolution of a few deformable models over the edges of the ROIs, thanks to action-reaction forces, even in presence of broken edges. However, they face another problem; the inability to “synchronize the evolution of a large number of concurrent models”. “Leaking” in this case occurs because the elastic models face different resistance along the path and arrive at the edges of the ROIs out of synchronism, as shown by arrows in Figure 13c. A problem that becomes worse when the number of expanding elastic models tends to increase.

The design of IDMSA took into account all the above-mentioned problems. From the perspective of “edge extraction by region-growing” the most important points of an image are precisely those located inside a narrow band (few pixels wide), around the “real” boundaries of the ROIs. By “real” we mean the set of candidate points that may represent in the image, the boundaries of the real objects. However, the “external” points also play a role in IDMSA. They serve as the arena for freely evolving models to fit themselves to the boundaries of this band. By letting unlabeled elastic model to grow and merge freely, before they reach the band, IDMSA introduces a powerful automatic merging mechanism for all non-significant (and not yet labeled) models, irrespective of the number of markers per ROI. This mechanism also avoids that local non-significant obstacles, as may occur in the Level-Set, Watershed or Seeded Region Growing paradigms, trap the elastic models. In addition, simple rules embedded into the growing and shrinking movements allow fine adjustment of the elastic models to the boundaries of the band, therefore reducing the possibility of leaking through ill-defined edges or growing parallel to them. Once inside the band, the labeled models follow an ever-growing movement, until they come to full stop close to edges of the regions, therefore assuring an automated stop criterion. To assure the convergence of models until they reach the idempotence condition, each image point and its immediate neighborhood are visited at least once during the evolution.

As IDMSA does not take into account the topographic information to guide the expanding process, the final location of the elastic model may not coincide exactly with the expected boundary of the object, as shown in Figure 13c. Nevertheless, to improve the final position of the edges, within the desired accuracy, IDMSA resorts to interactivity, which gives the user the possibility to insert information of higher semantic content into the processes. Interactivity allows changing the set of markers, including their number, size and shape, the EB thickness and the parameters controlling action and reaction movements.

Integer arithmetic implementation assures IDMSA fast execution times, a significant improvement when compared to Level-Sets, which require the computation of a large number of differentials in floating-point. In addition, IDMSA does not resort to the sophisticated set of wait queues required by immersion simulation methods. IDMSA execution time depends on the density, size and position of markers. Lower densities imply longer execution time since the models will take more iterations to converge. If a linear labeling algorithm is used [11] the overall algorithm time complexity will be linear, i.e., $O(N)$, since morphological erosion, dilation as well as edge detection by scanning a labeled image are all linear time algorithms.

5. Conclusions and Outlook

Designed and implemented to fulfill the requirements of a typical material characterization procedure, IDMSA focus particularities of images grabbed at microscopic and nanoscopic scale under unfavorable conditions, as a large number of small objects in a single image field, delimited by ill-defined boundaries.

Although designed to explore interactivity, IDMSA may allow fully automated execution, in batch mode, for a large number of similar images of a given class, if a denoising sequence could extract the required set of markers for that class of image. Extension of the IDMSA algorithm to 3D images is straightforward since all operations and algorithms involved are promptly convertible from 2D to 3D realm.

The several examples of real applications presented in the text show that IDMSA is a viable alternative to small-scale image segmentation.

Acknowledgments

The author acknowledge the financial support of XXXX (Grant CEX-APQ-00309).

References

- [01] F. Meyer. Un algorithme optimal de ligne de partage des eaux. In: *Proceedings of the VIII Congrès de Reconnaissance de Forme et d'Intelligence Artificielle*. Lyon, France, 847-857, 1991.
- [02] L. Vincent, P. Soile. Watershed in Digital Spaces: an efficient algorithm based on immersion simulations. *IEEE Transactions on Pattern Analysis and Machine Intelligence*, 13, 6, 583-598, 1991.
- [03] S. Osher, and J. A. Sethian. Fronts Propagating with Curvature-Dependent Speed: Algorithms Based on Hamilton Jacobi Formulations, *Journal of Computational Physics*, 79, 12-49, 1988.
- [04] J. A. Sethian. *Level Set Methods and fast Marching Methods*, Cambridge University Press, Cambridge, 2000.
- [05] R. Malladi, et al. Shape modeling with front propagating: a level set approach. *IEEE Transactions on Pattern Analysis and Machine Intelligence*, 17, 2, 158-175, 1995.
- [06] G. Papari, N. Petkov. Edge and line oriented contour detection: State of the Art. *Image and Vision Computing*, 29, 79-103, 2011.
- [07] J. Serra. *Image Analysis and Mathematical Morphology*, Academic Press, London, 1982.
- [08] M. Grimaud. *La Geodesie Numerique en Morphologie Mathematique. Application a la Detection Automatique de Microcalcifications en Mammographie Numerique*. PhD Thesis, École Nationale Supérieure des Mines de Paris, Fontainebleau, France, 1991.
- [09] A. Yezzi. Modified curvature motion for image smoothing and enhancement. *IEEE Transactions on Image Processing*. 7, 3, 345-352, 1998.
- [10] X. Xu. A method based on rank-ordered filter to detect edges in cellular image. *Pattern Recognition Letters*. 30, 6, 634-640, 2009.

- [11] F. Chang, et. al. 2004. A linear-time component-labeling algorithm using contour tracking technique. *Computer Vision and Image Understanding*, 93, 206-220, 2004.
- [12] R. Gonzalez, R. Woods. *Digital Image Processing*, Prentice Hall, New Jersey, 2001.
- [13] J. A. T. Pigatto, et. al. Morphometric analysis of the corneal endothelium of Yacare caiman (Caiman yacare) using scanning electron microscopy. *Veterinary Ophthalmology*. 7, 205-208, 2004.
- [14] R. Adams and L. Bischof. Seeded Region Growing. *IEEE transactions on Pattern Analysis and Machine Intelligence*, 16, 6, 641-647, 1994.
- [15] B. McCarey et al. Review of Corneal Endothelial Specular Microscopy for FDA Clinical Trials of Refractive Procedures, Surgical Devices, and New Intraocular Drugs and Solutions. *Cornea*, 27, 1, 2008.
- [16] T. Huang and X. Bai. An Improved algorithm for Medical Image Segmentation. Second International Conference on Genetic and Evolutionary Computing (Wgec). Y. Du (editor) IEEE Computer Society, 2009.
- [17] I. Levner and H. Zhang. Classification-Driven Watershed Segmentation. *IEEE Transaction on Image Processing*, 16, 5, 2007.
- [18] S. Colantonio et al. A Two-Step Approach for Automatic Microscopic Image Segmentation Using Fuzzy Clustering and Neural Discrimination. *Pattern Recognition and Image Analysis*, 17, 429-437, 2007.
- [19] A. Soufu and Petros Maragios. Generalized Flooding and Multicue PDE-Based Image Segmentation. *IEEE Transactions on Image Processing*. 17, 3, 2008.
- [20] B. Lu et al. Automated Grain Boundary detection Using the Level-Set Method. *Computers and Geosciences*, 35, 267-275, 2009.
- [21] E. Ribeiro and M. Shah. Computer Vision for Nanoscale Imaging. *Machine Vision and Applications*, 17, 147-162, 2006.
- [22] M. Hasanzadeh and S. Kasaei. A New Fuzzy Connectedness Relation for Image Segmentation. 3th International Conference on Information and Communication Technologies: From Theory to Applications, 1-6, 2008.